Southwest Nova Scotia
Tidal Energy Resource Assessment
Volume 2:
Numerical Modelling of Digby Neck Tidal Currents

Mitchell O-Flaherty-Sproul[1] and Richard Karsten[1]

June 24, 2013

[1]**Acadia University**

Contents

List of Figures

List of Tables

Chapter 1

Introduction

For the Numerical Modelling part of the Project, the goal was to complete high-resolution 2D and 3D numerical simulations of tidal flow in the Digby Neck region that could be validated through comparison to the flow and water level observations collected from ADCPs and pressure sensors, respectively. Through the validation procedure, the numerical model would be improved to better capture the higher frequency variation in the tidal currents seen in the ADCP records. Finally, using this model and the comparison to ADCP data, estimates of the potential power that could be extracted from the passages could be improved and put into better context.

As described below, the spatial grid used in the numerical model was adapted to include much higher resolution in the three Digby Neck passages. The model uses the high-resolution bathymetry gathered as part of this project and the numerical grid was adapted to better represent the coastlines. These adaptations produce a model grid with a 10-15 m spatial resolution in the passages, approaching the scale of TECs.

The focus of the project was the validation of the refined numerical model. Therefore this chapter describes these comparisons in some detail. At almost all locations, the surface elevation in numerical simulations is nearly identical to the ADCP or RBR pressure measurements from that location. For the velocity, the comparison of the numerical simulations to the ADCP data focused on the 2D, depth averaged velocity. The majority of the ADCP and numerical results indicate that the tidal flow is barotropic, that is, it does not change direction with depth. Therefore, the depth-average flow captures the most important characteristics of the flow, the changes of the flow in time. Also, long-time 2D numerical simulations are computationally feasible since 40-day-long simulations that overlap each of the ADCP simulations can be completed in less than one week. In contrast, only short 3D simulations have been completed and these results are not discussed here. The comparison of the high-resolution numerical simulations to the ADCP time series has been very positive. In locations with strong tidal flow, the numerical model is capturing the major characteristics of the tidal flow, including the magnitude of the speed, the direction of the flow and the asymmetry between flood and ebb. As well, the refinement of the model grid allows the simulation of high frequency variations in the flow. The model correctly predicts when and where such fluctuations occur, but over predicts their maginitude. In Digby Gut, the simulated

tidal flow is ebbing for a longer time than it is flooding. This asymmetry is not present in the ADCP data and the reason for this discrepancy has not been determined.

The numerical model is used to briefly examine the power potential of the Digby Neck passages. The 2D numerical simulations were adapted to extract power from the flow using full fences that extended across each passage following [Karsten, McMillan, Lickley, and Haynes, 2008]. The power extracted is plotted versus the resulting flow reduction for each of the passages. These calculations demonstrated the large difference in potential power for a passage that lies between two large bodies of water (Grand and Petit Passages) and one that connects a bay to the ocean (Digby Gut). As discussed, the results of these theoretical power calculations must be carefully interpreted as small variations in current speeds produce large variations in power. As well, the estimates are based on large numbers of turbines extracting power from the mean flow, not a few turbines placed strategically in high flow locations.

Chapter 2

The Numerical Model

For the calculations in this report, we simulated the tides and currents in the Bay of Fundy using the Finite Volume Coastal Ocean Model (FVCOM) [Chen, Beardsley, and Cowles, 2006]. The model grid was adapted from a grid developed by David Greenberg and Jason Chaffrey at the Bedford Institute of Ocean Sciences. The model domain covers the entire Gulf of Maine and Bay of Fundy with its open boundary beyond the continental shelf. The model is forced by specifying the tidal amplitude and phases of five tidal constituents at the open boundary (see Table 2.1) . The model has been previously validated through comparisons to tide gauge data various locations around the Bay of Fundy. A further discussion of the numerical model can be found in [Karsten et al., 2008, Karsten, 2011, Karsten, O'Flaherty-Sproul, McMillan, Culina, Trowse, and Hay, 2012, Karsten, Swan, and Culina, 2013].

Tidal Constituant	Amplitude Range (cm)
M_2	38.5 – 52.0
S_2	7.8 – 12.8
N_2	8.2 – 12.2
K_1	1.9 – 11.5
O_1	1.9 – 10.9

Table 2.1: The 5 tidal constituents that are used to force the numerical simulations. The amplitude and phase of these constituents are specified at each node on the open boundary of the model grid.

2.1 Grid Refinement

The development of the model grid was undertaken as part of Mitchell O'Flaherty-Sproul's MSc thesis where it is described in detail. Here we give a brief overview of the grid characteristics. The original BIO grid was initially adapted to include the three Digby Neck Passages with a grid that had a resolution of 100 m to 200 m in the

three passages. This low resolution grid was used to establish the tidal flow through the passages. The spacial resolution was large in comparison to an the diameter of a TEC device. This was sufficient for calculating initial net power estimates. From initial comparison to ADCP data it was clear that this resolution was insufficient to model the fluctuations seen in the tidal currents, especially those seen downstream of major bathymetric features such as headlands and islands.

The resolution of the grid was increased until the element side length was averaging between 10 and 20 meters in each of the three passages. This required approximately 30,000 nodes in each passage. The resolution was also increased in the south-west Brier Island region to resolve numerical errors that were caused by steep bathymetry in that region. The resolution was limited to the 10 m range for three reasons. First, the grid size was similar to the expected TEC scale and therefore could be used for site characterization. Second, flow at scales less than 10 m will involve turbulent, non-hydrostatic dynamics which FVCOM was not designed to model.

Finally, the model simulations discussed in this report are only 2D, depth-averaged simulations. The model has been run in 3D mode, with 10 sigma-layers. However, using this high-resolution grid, these simulations are taking longer than real time to run, making month-long simulations unfeasible. Furthermore, the main advantage of using a 3D barotropic model is the proper representation of the vertical profile of the flow. In most strong tidal flows, the vertical profile of the flow satisfies a logarithmic profile, consistent with a law-of-the wall boundary layer. In such flows, death-averaged simulations do a very good job of representing the horizontal variation of the flow. In the some of the ADCP data, the vertical profiles vary from a simple logarithm. It is not clear what causes this variation and our initial 3D models have not replicated it. Therefore, at this time, the 3D simulations are offering little additional insight into the flow dynamics. As shown in this report, the high-resolution grid does capture many important spatial variations in the flow that are not modelled at lower resolution, for example, the flow variations around Peter Island,. The 2D simulations can also be used for initial estimates of the power that can be extracted from the passages. Therefore, we have decided to focus solely on the high-resolution 2D simulations in this report, and leave the 3D simulations for continuing research.

Table 2.2 contains the detailed grid metrics for the original grid as well as the two grids developed. Figure **??** shows the maximum side length in meters of each element in Grand Passage for both the Low Resolution and High Resolution grids.

	Original Grid	Low Resolution	High Resolution
Nodes	5261	11224	107318
Elements	9300	20388	209711
Side Length: Max (m)	68926.4	64370.9	64370.9
Side Length: Min (m)	334.97	26.96	6.375
Time-Step: 2D (s)	18.0	2.0	0.95

Table 2.2: Statistic for the two grids that were created to model the Digby Neck passages. The results descrybed in the remainder of the report are for the High Resolution grid.

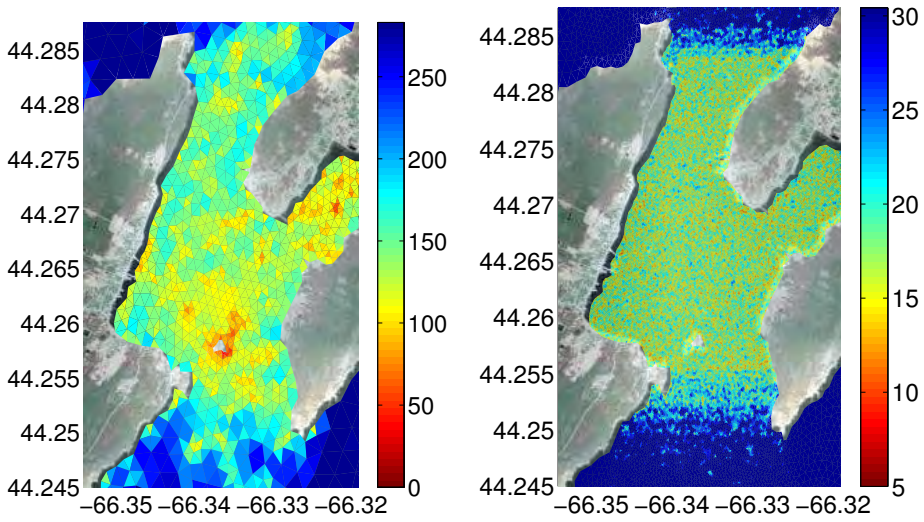

(a) Grand Passage (b) Grand Passage

Figure 2.1: Element side length in (a) Low Resolution and (b) High Resolution model for Grand Passage. Color denotes in meters the maximum side length of each element.

2.2 Bathymetry

The dynamics of tidal flow is dominated by the bathymetry, and therefore a numerical model's results are only as accurate as the bathymetry data it uses. For the simulations discussed here, high resolution bathymetry data in each of the three passages and Annapolis Basin was required.

Within the model grid, the bathymetry is set by assigning each node a mean water depth. All nodes, including those that wet and dry require an accurate water depth. This causes some difficulty as water depths in the intertidal zone are difficult to measure. Furthermore, bathymetric data sets used for navigation often list the low-low water depth and have to be appropriately adjusted to give the mean water depth required in the numerical model. We used ten different sources of bathymetric data to develop our final grid:

1. scotMaine: the original grid, used to baseline the redepthed mesh to insure at least the old level of bathymetric accuracy.

2. ufcombGT-10_95mBcor.lld: depth data that covers the upper Bay of Fundy, obtained from the Bedford Institute of Oceanography.

3. Digby Gut, Ricom: data extracted from another grid obtained from Triton Environmental Consultants Ltd., used to fill data gaps in Digby Gut.

4. South West Brier Island - CHS: data covering the south west area of Brier Island, obtained from Canadian Hydrographic Service.

5. Petit Passage - CHS: data covering Petit Passage, obtained from Canadian Hydrographic Service.

6. Digby Passage - CHS: data covering Digby Passage, obtained from Canadian Hydrographic Service.

7. Grand Passage - CHS: data covering Grand Passage, obtained from Canadian Hydrographic Service.

8. Annapolis Basin - Olex: data covering the Annapolis Basin, obtained from Olex software as part of the Project.

9. Grand Passage - Olex: data covering Grand Passage, gathered as part of the Project.

10. Petit Passage - Olex: data covering Petit Passage, gathered as part of the Project.

The data sets are listed in order from the least accurate/lowest resolution to the most accurate/highest resolution. The grids bathymetry is initially set to the depth given by dataset 1. The bathymetry is refined by sequentially using the remaining datasets. The bathymetry is set to the value of the dataset at all nodes that lie in the domain of the dataset.

The bathymetry data gathered as part of the Project has vastly improved the accuracy of the bathymetry in the model, resulting in much better agreement between modelled tidal currents and the ADCP measurements. Further improvements in the bathymetry in Digby Gut and Annapolis Basin are still required to complete this process.

For the simulations reported on here, the model uses a constant bottom friction coefficient , 2.5×10^{-3}, throughout the domain. The bathymetry data has indicated that the bottom roughness varies in the three passages. The drag coefficient estimated from the ADCP data also indicated that it varies in space, but also with the ebb and flood tides! The inclusion of variable bottom roughness may address some of the discrepancies between the model and ADCP data that are described below. However, the inclusion of variable bottom roughness in a high-resolution model is not trivial – the scheme must properly balance the resolved form drag and the unresolved roughness. This analysis is best done in a 3D model of the passages, where vertical profiles can be compared to ADCP profiles, and requires more data from the bottom boundary layer in the three passages. This is ongoing work.

Chapter 3

Model Comparison to ADCP data

In this section we describe the comparison of the numerically modelled tidal currents to flow and water level observations (ADCP and pressure sensor data) gathered as part of the Project. Our goal is to validate the model and identify possible improvements and limitations. In all, we compare model predictions to 12 ADCPs: 3 in Grand Passage, 4 in Petit Passage, and 5 in Digby Gut. For each ADCP location, we provide a plot comparing the depth averaged tidal velocities and water levels. Note that we did not complete a comparison for ADCP at location 2 in Grand Passage because we did not have the direction of the flow for that data set. In these plots u is the east/west speed (east positive) and v is the north/south speed (north positive). A table is provided for each passage showing the predicted and observed flow statistics..

3.1 Comparison to Grand Passage ADCPs

The locations of the 3 ADCPs in Grand Passage used for comparison are shown in Figure 3.1 along with the model bathymetry. Figures 3.2, 3.3 and 3.4 shows plots of model predicted and observed velocities. Table 3.1 provides a side-by-side comparison of the flow statistics.

In general, there is reasonable agreement between the ADCP data and the simulation data at these three locations. When there is strong tidal flow, such as at ADCP location 4, the model results capture the main characterizations of the ADCP velocities. The magnitude and direction of the velocity is well modelled and we see the fluctuation in the velocity when the flow is strongest. ADCPs 3 and 5 were placed at locations to capture the turbulent flow in the wake of Peter's Island. Considering this, the model again has reasonable agreement. It clearly simulates turbulent flow at the same time as the ADCP data indicates there is turbulent flow. At all locations, the model predicts larger variations when the flow is turbulent.

There are clear differences in Table 3.1 between the ADCP data and model data statistics. Once again the model data best agrees with the ADCP data at ADCP location

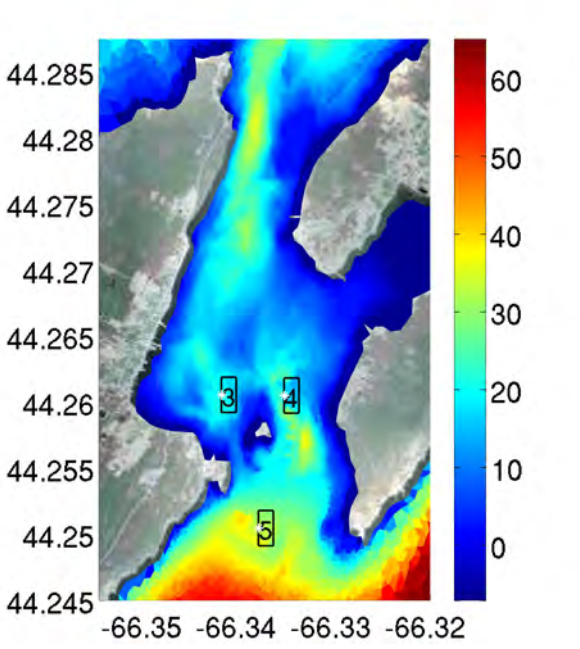

Figure 3.1: The locations of the 3 ADCPs deployed in Grand Passage. The markers show the locations of the ADCPs the colors show the depth of the water. The numbers on the markers correspond to the ADCPs designation.

Site	ADCP 3	Model 3	ADCP 4	Model 4	ADCP 5	Model 5
Velocity						
Mean speed (m/s)	0.40	0.51	1.67	1.74	0.38	0.53
Maximum speed (m/s)	1.10	2.60	2.86	2.87	1.28	2.82
Ebb/flood asymmetry	0.83	1.24	0.97	1.03	0.93	1.04
Power						
Mean kin. power den. (kW/m^2)	0.06	0.18	3.39	3.82	0.06	0.20
Kinetic power asymmetry	0.65	3.71	0.86	1.08	1.32	1.98
Direction						
Principal direction (heading)	16	-10	-6	-18	12	265
Directional deviation (deg)	66	41	12	8	27	45
Directional asymmetry (deg)	118	30	8	11	64	60

Table 3.1: Table comparing tidal flow statistics for ADCP data and numerical model interpolated to the Grand Passage ADCP locations.

4. The agreement of the statistics at sites 3 and 5 is not very good. This is not surprising giving the highly variable flow at these locations and that the model is predicting a higher level of variability. In cases of strongly variable flow, the simple statistics presented in this table must be considered cautiously. The numerical data used for these calculations is an instantaneous prediction of the water velocity and not an ensemble average like that used for the ADCP data. A more careful comparison would generate a high frequency time series of numerical data and calculate an ensemble average of the data in a similar manner to that used to analyze the ADCP data. Furthermore, in regions of turbulent flow a more careful analysis of the flow statistics of a highly variable time series is required to determine if the numerical model is capturing the characteristics of the large-scale variations in the flow. This is ongoing research.

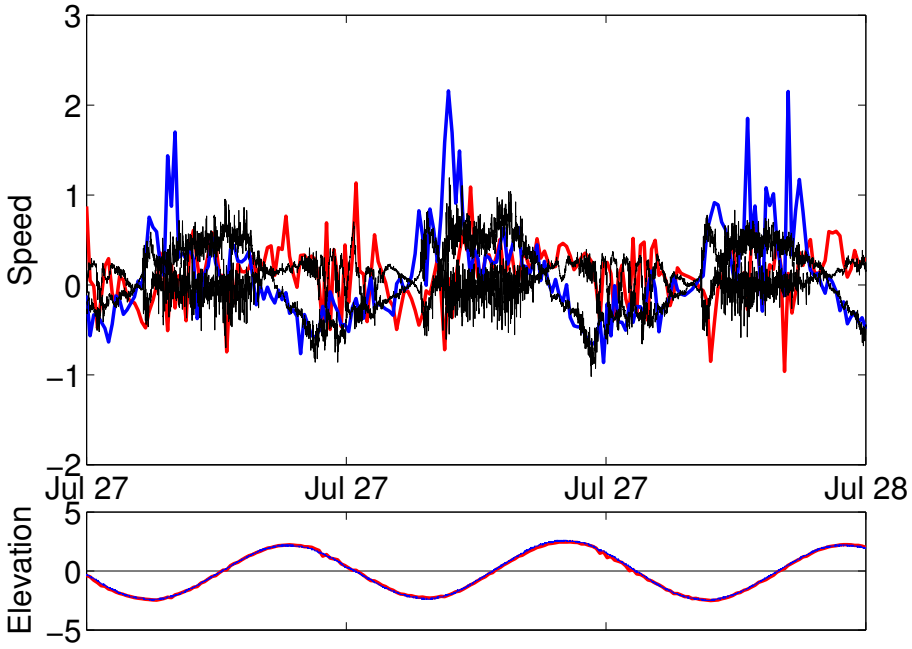

Figure 3.2: Comparison between Grand Passage ADCP 3 and model velocities in m/s. The ADCP data are the black curves and the model data the coloured curves, blue for u and red for v. The lower plots are the surface elevation in metres, for both the model and ADCP.

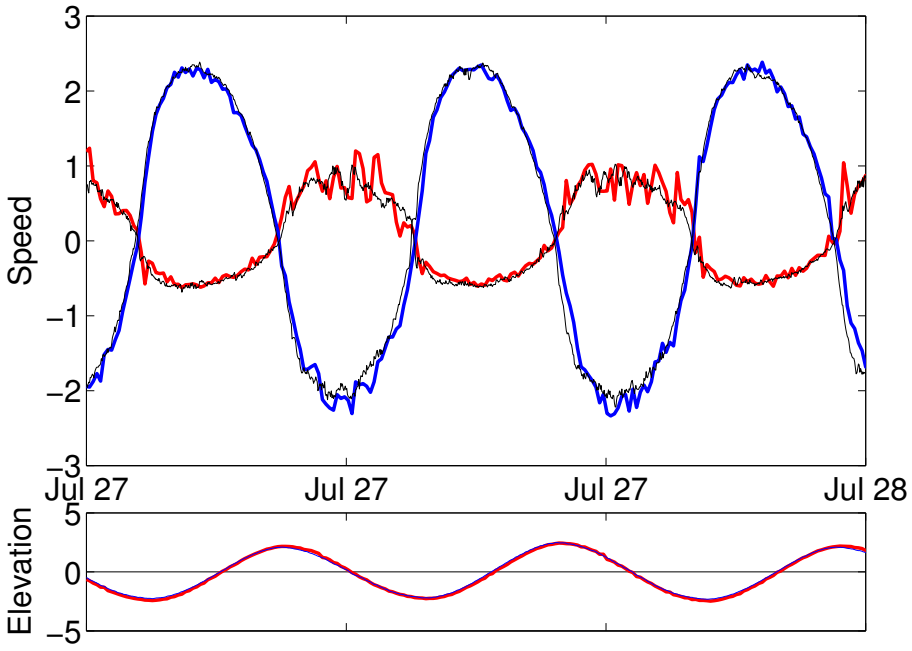

Figure 3.3: Comparison between Grand Passage ADCP 4 and model velocities in m/s. The ADCP data are the black curves and the model data the coloured curves, blue for u and red for v. The lower plots are the surface elevation in metres for both the model (red) and ADCP (blue).

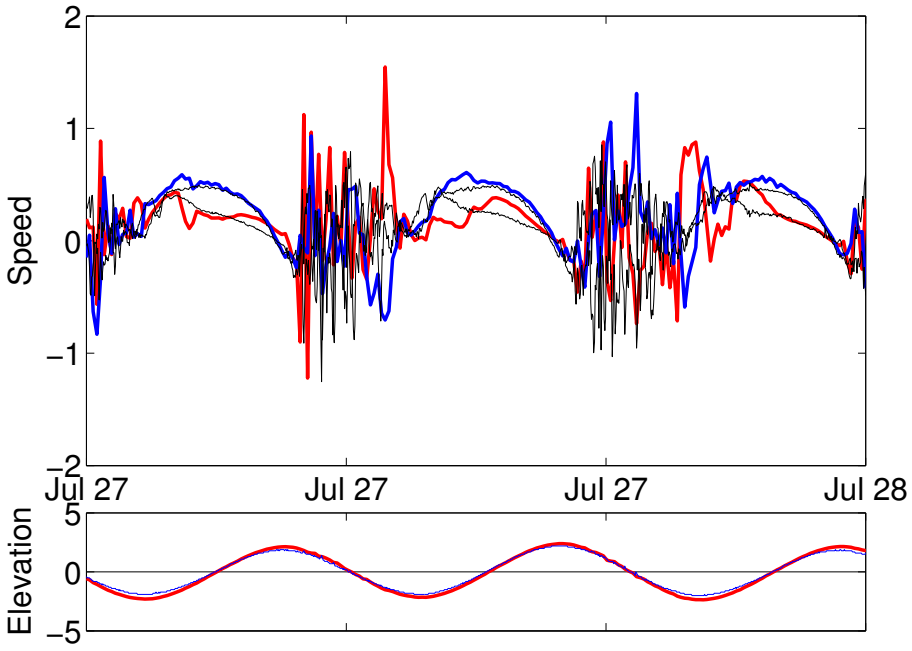

Figure 3.4: Comparison between Grand Passage ADCP 5 and model velocities in m/s. The ADCP data are the black curves and the model data the coloured curves, blue for u and red for v. The lower plots are the surface elevation in metres for both the model (red) and ADCP (blue).

3.2 Comparison to Petit Passage ADCPs

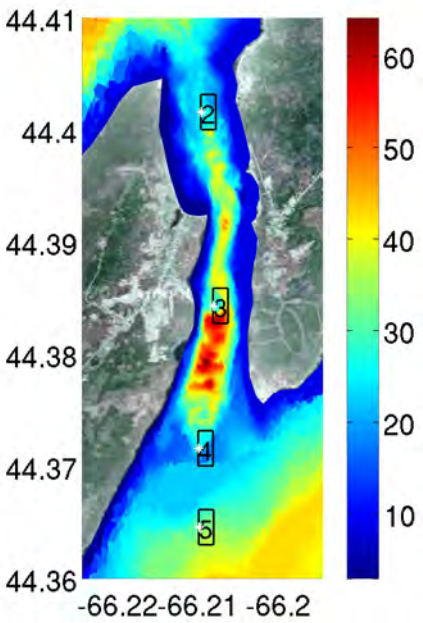

Figure 3.5: The locations of the 4 ADCPs deployed in Petit Passage. The markers show the locations of the ADCPs the colors show the depth of the water. The numbers on the markers correspond to the ADCPs designation.

The locations of the 4 ADCPs in Petit Passage used for comparison are shown in Figure 3.5 along with the model bathymetry. Figures 3.6, 3.7, 3.8 and 3.9 shows plots of ADCP and model velocities. Table 3.2 provides a side-by-side comparison of the flow statistics.

Overall, the model is doing a reasonable job at replicating the flow through Petit Passage. The model is predicting stronger flow on the ebb tide. Once again, the model is predicting velocity fluctuations at the correct location and time, but with too large a magnitude. The combination of these two results in much higher maximum velocities and power densities. Again, this emphasizes how small errors in the flow can be translated into large discrepancies in some of the statistics.

Site	ADCP 2	Model 2	ADCP 3	Model 3	ADCP 4	Model 4	ADCP 5	Model 5
Velocity								
Mean speed (m/s)	1.79	2.06	1.91	2.12	1.06	1.29	0.51	0.66
Maximum speed (m/s)	3.41	3.68	3.83	5.70	2.73	3.51	1.71	3.17
Ebb/flood asymmetry	0.95	0.97	1.41	0.74	1.61	0.51	1.77	0.36
Power								
Mean kin. power den. (kW/m^2)	4.39	6.72	5.86	7.99	1.17	2.36	0.17	0.62
Kinetic power asymmetry	0.78	0.90	2.81	0.36	4.89	0.12	7.98	0.03
Direction								
Principal direction (heading)	3	-17	16	9	25	9	34	9
Directional deviation (deg)	8	7	49	6	35	9	20	21
Directional asymmetry (deg)	9	3	82	5	29	11	18	10

Table 3.2: Table comparing tidal flow statistics for ADCP data and numerical model interpolated to the Petit Passage ADCP locations.

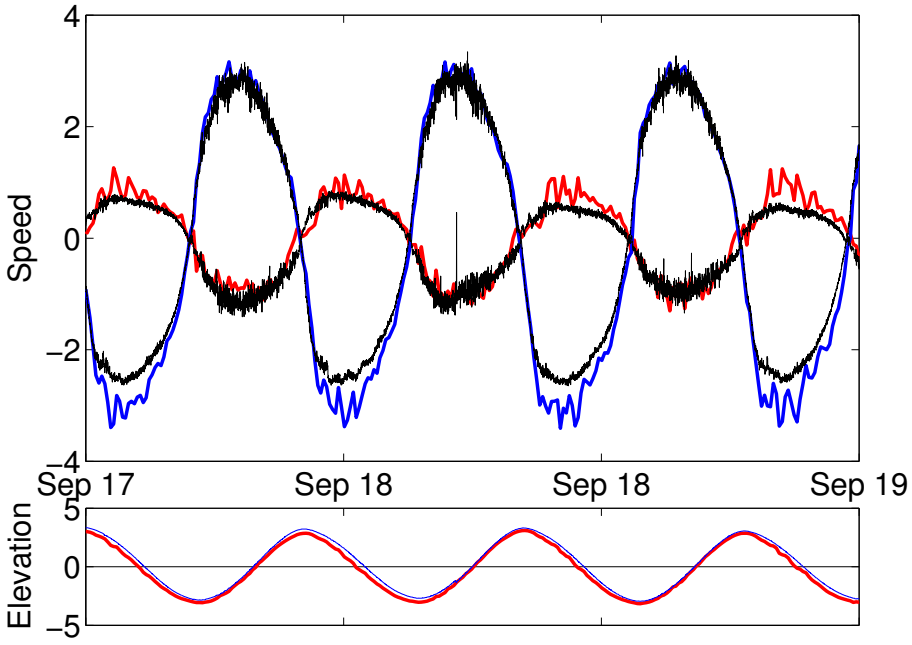

Figure 3.6: Comparison between Petit Passage ADCP 2 and model velocities in m/s. The ADCP data are the black curves and the model data the coloured curves, blue for u and red for v. The lower plot are the surface elevation in metres, for both the model (red) and ADCP (blue).

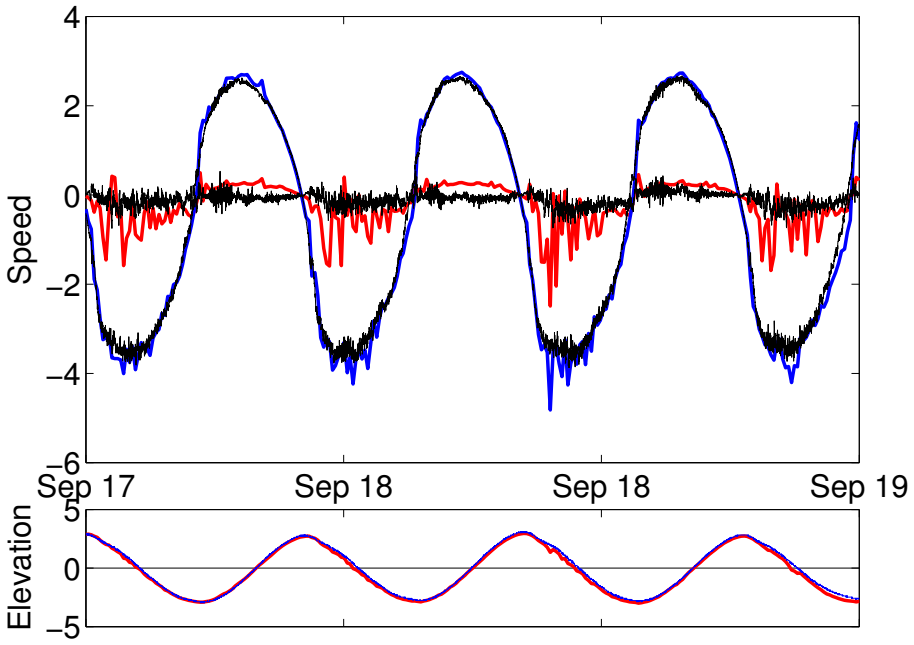

Figure 3.7: Comparison between Petit Passage ADCP 3 and model velocities in m/s. The ADCP data are the black curves and the model data the coloured curves, blue for u and red for v. The lower plot are the surface elevation in metres for both the model (red) and ADCP (blue).

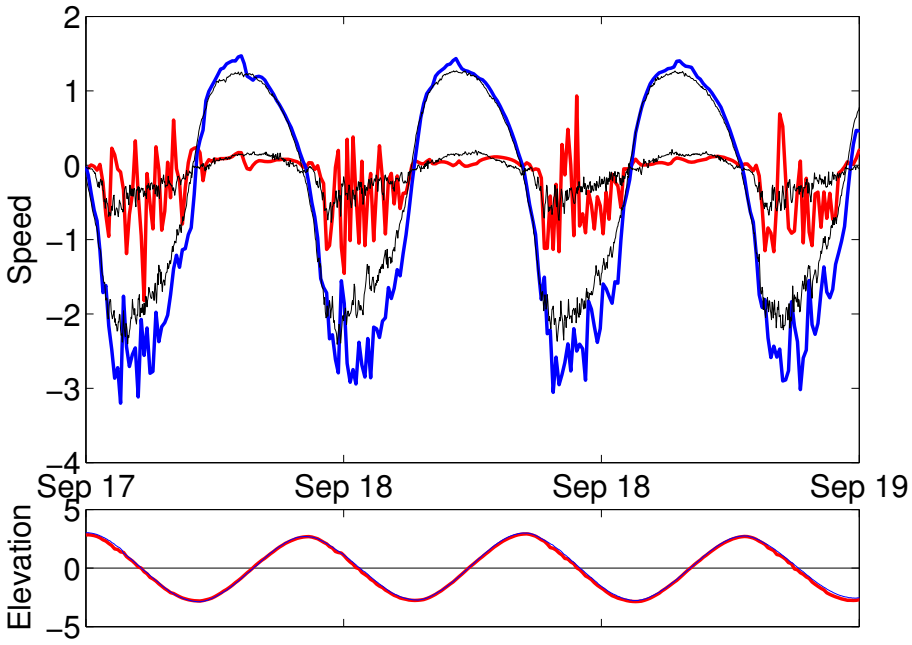

Figure 3.8: Comparison between Petit Passage ADCP 4 and model velocities in m/s. The ADCP data are the black curves and the model data the coloured curves, blue for u and red for v. The lower plot are the surface elevation in metres for both the model (red) and ADCP (blue).

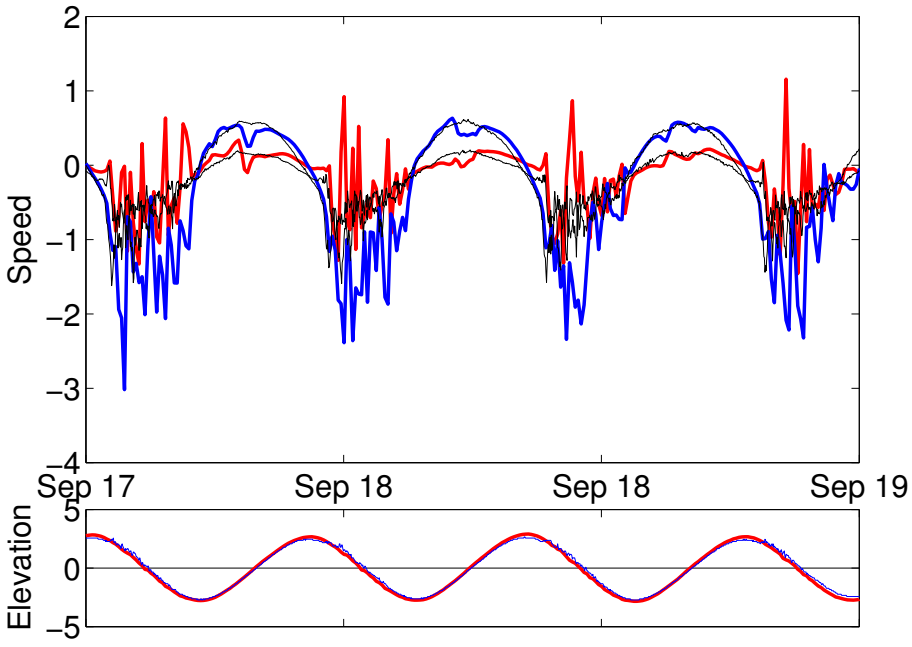

Figure 3.9: Comparison between Petit Passage ADCP 5 and model velocities in m/s. The ADCP data are the black curves and the model data the coloured curves, blue for u and red for v. The lower plot are the surface elevation in metres for both the model (red) and ADCP (blue).

3.3 Comparison to Digby Gut ADCPs

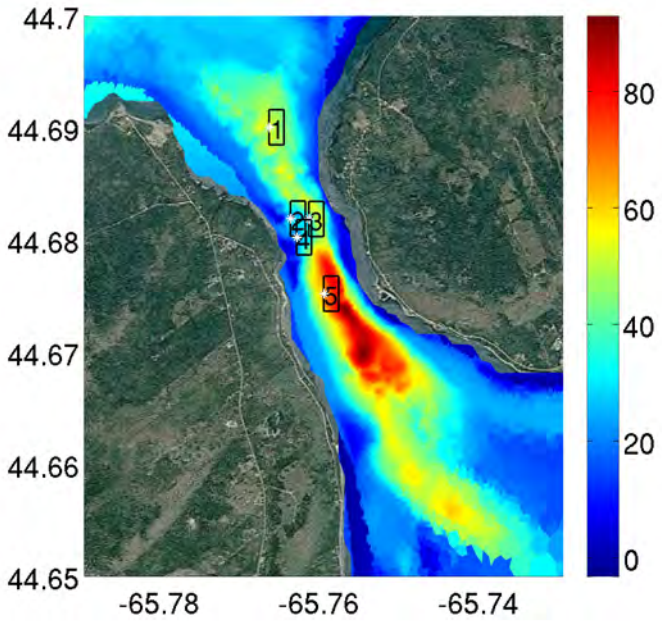

Figure 3.10: The locations of the 5 ADCPs deployed in Digby Gut. The markers show the locations of the ADCPs the colors show the depth of the water. The numbers on the markers correspond to the ADCPs designation.

The locations of the 5 ADCPs in Digby Gut used for comparison are shown in Figure 3.10 along with the model bathymetry. Figures 3.11, 3.12, 3.13, 3.14 and 3.15 shows plots of ADCP and model velocities. Table 3.3 provides a side-by-side comparison of the flow statistics.

The comparison for Digby Gut is the poorest of the three passages. The model is under predicting the speed at all locations. The phase is also being delayed during the ebb tide, thus the model's max speed is peaking late for ebb tide. This indicates a fundamental problem with the model flow through Digby Gut that is likely connected to the bathymetric data used for Digby Gut and Annapolis Basin. Since the flow through Digby Gut is directly related to the tides in Annapolis Basin, the tides in the entire region must be modelled accurately to get the flow correct. While the figures clearly show discrepancies between the model and ADCP velocities, the flow statistics downplay this difference. However, they do show that the model is underestimating the power density by a factor of 2.

Site	ADCP 1	Model 1	ADCP 2	Model 2	ADCP 3	Model 3	ADCP 4	Model 4	ADCP 5	Model 5
Velocity										
Mean speed (m/s)	0.87	0.58	1.20	0.88	1.34	1.00	1.27	0.90	0.67	0.46
Maximum speed (m/s)	2.15	2.22	2.65	2.60	2.95	2.50	2.74	2.72	1.49	1.79
Ebb/flood asymmetry	1.24	0.95	0.91	0.84	0.90	1.05	1.01	0.83	1.17	0.83
Power										
Mean kin. power den. (kW/m^2)	0.65	0.24	1.54	0.73	2.18	1.08	1.79	0.81	0.26	0.11
Kinetic power asymmetry	2.01	0.58	0.76	0.71	0.72	1.13	1.07	0.72	1.85	0.53
Direction										
Principal direction (heading)	-25	-24	-11	-21	-18	-21	-37	-29	-16	-21
Directional deviation (deg)	11	14	13	7	18	7	6	6	26	26
Directional asymmetry (deg)	30	22	8	2	6	3	6	9	23	5

Table 3.3: Table comparing model data to Digby Gut ADCP data.

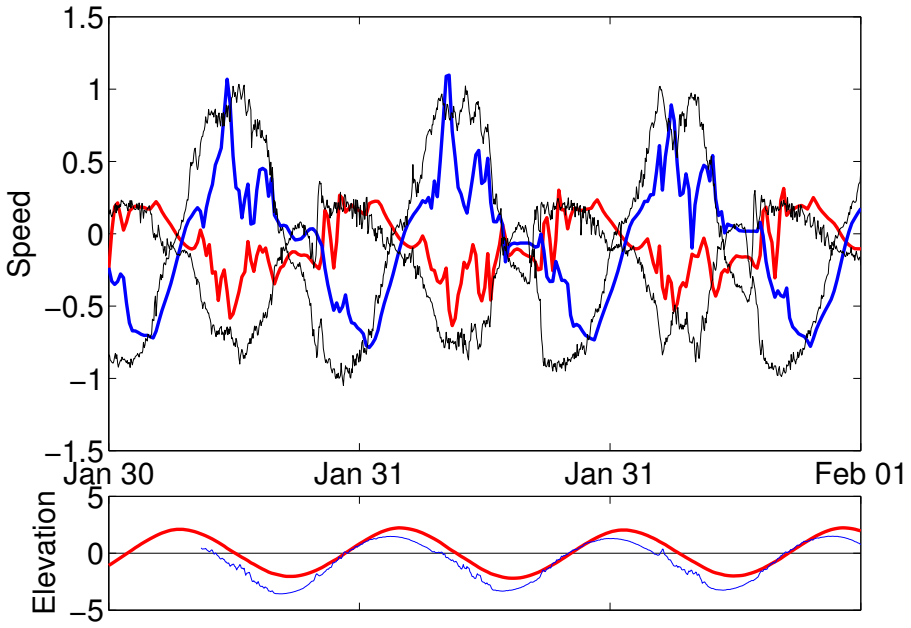

Figure 3.11: Comparison between Digby Gut ADCP 1 and model velocities in m/s. The ADCP data are the black curves and the model data the coloured curves, blue for u and red for v. The lower plots are the surface elevation in metres for both the model (red) and ADCP (blue).

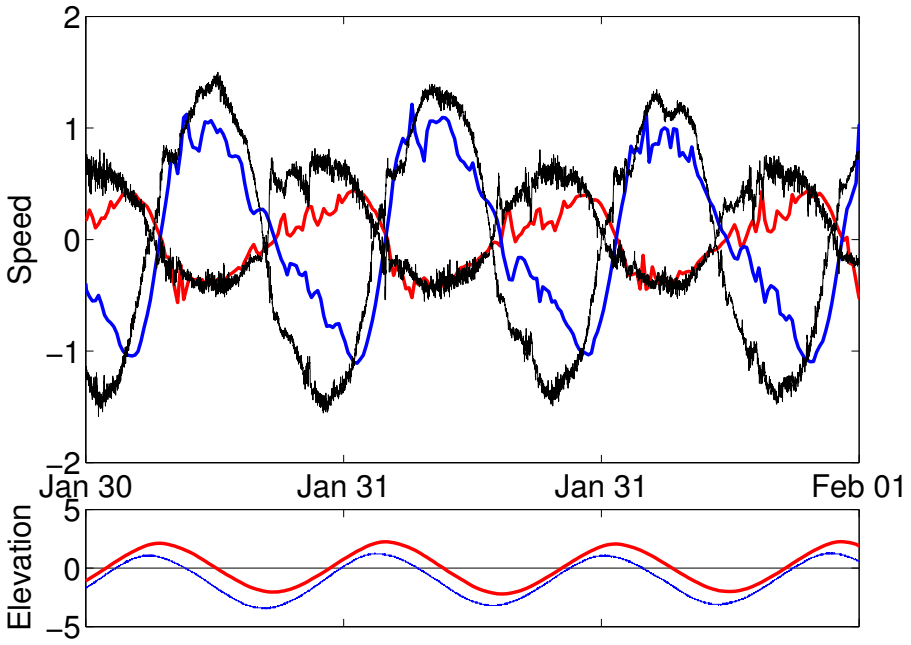

Figure 3.12: Comparison between Digby Gut ADCP 2 and model velocities in m/s. The ADCP data are the black curves and the model data the coloured curves, blue for u and red for v. The lower plots are the surface elevation in metres for both the model (red) and ADCP (blue).

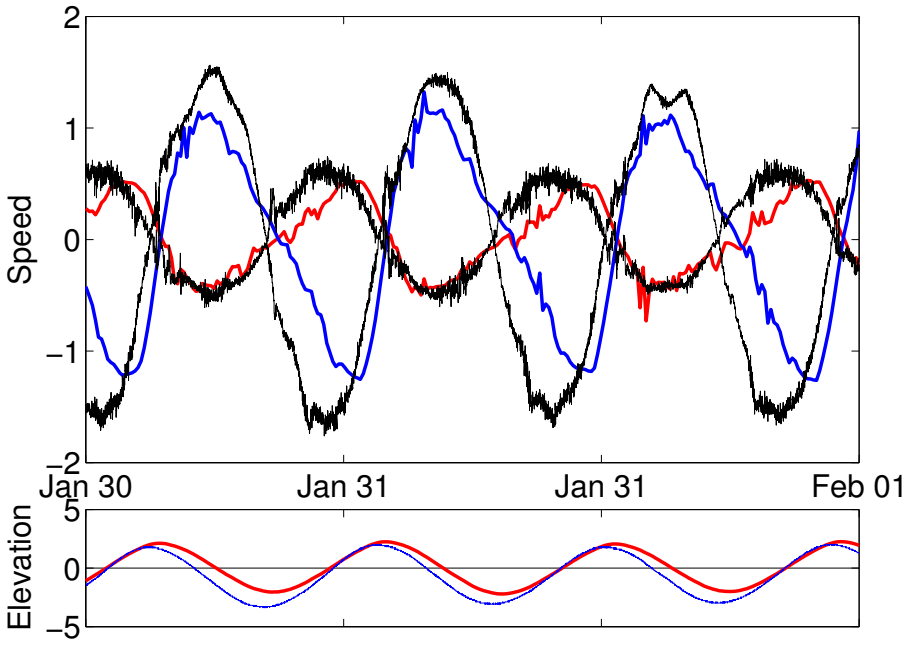

Figure 3.13: Comparison between Digby Gut ADCP 3 and model velocities in m/s. The ADCP data are the black curves and the model data the coloured curves, blue for u and red for v. The lower plots are the surface elevation in metres for both the model (red) and ADCP (blue).

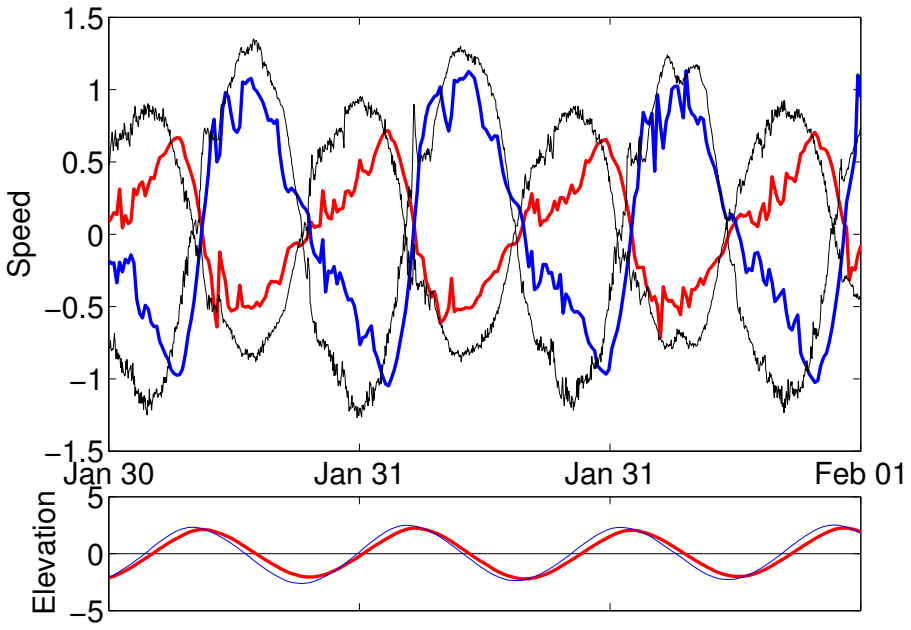

Figure 3.14: Comparison between Digby Gut ADCP 4 and model velocities in m/s. The ADCP data are the black curves and the model data the coloured curves, blue for u and red for v. The lower plots are the surface elevation in metres for both the model (red) and ADCP (blue).

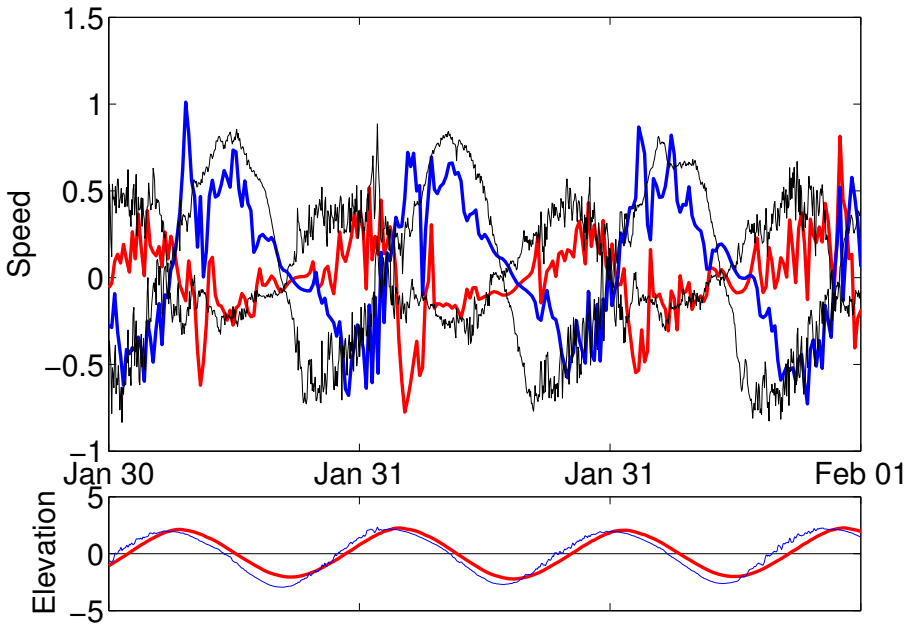

Figure 3.15: Comparison between Digby Gut ADCP 5 and model velocities in m/s. The ADCP data are the black curves and the model data the coloured curves, blue for u and red for v. The lower plots are the surface elevation in metres for both the model (red) and ADCP (blue).

Chapter 4

Explaining Variation in the Flow

One advantage of numerically modelling the flow is that the variations seen in the time-series can be connected to spatial variations in the flow and, thus, more directly related to physical processes. In order to highlight the variation in the flow, we decompose the flow into two components:

1. the tidal flow: the portion directly related to the forcing tidal constituents as calculated using t_tide [Pawlowicz, 2001]

2. the intra-tidal or residual flow: the flow variations that are more directly connected to the local bathymetry, calculated as the total flow minus the tidal flow.

This can be done at every point on the numerical grid to produce a spatial map of the tidal and intra-tidal flow. The result of this process is illustrated in Figures 4.1 , 4.2 and 4.3 The maps of the intra-tidal flow clearly indicate the strong influence of Peter's Island on the downstream flow.

From these maps, we can reach several conclusions. First, the modelled intra-tidal flow is similar in magnitude to the tidal flow and therefore critical in characterizing the flow. The intra-tidal flow is very asymmetric with ebb and flood tide. The modelled velocity fluctuations seen at ADCP location 3 during the flood tide and ADCP location 5 during the ebb tide are connected to eddies being shed of Peter's Island. Since the ADCP data showed similar fluctuations, we expect that this intra-tidal flow is being modelled realistically (although the amplitude is too high). It should be noted that the details of the intra-tidal flow only became apparent in the numerical simulations when the grid had sufficient number of elements to resolve these flow structures.

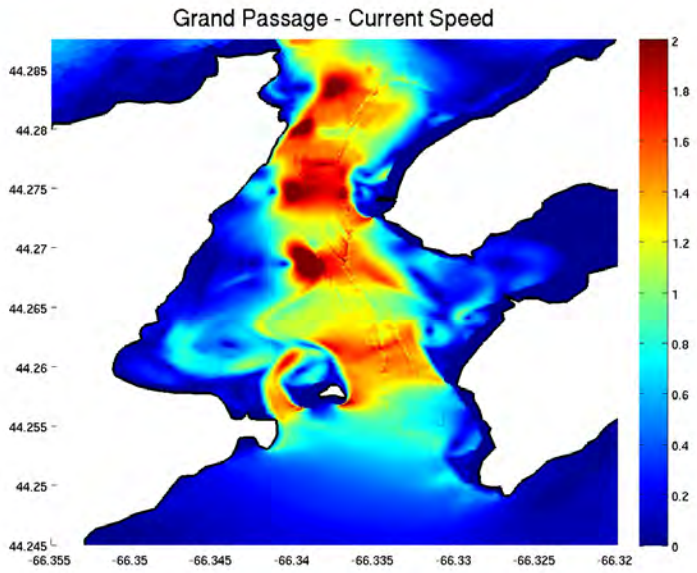

(a) Complete speed

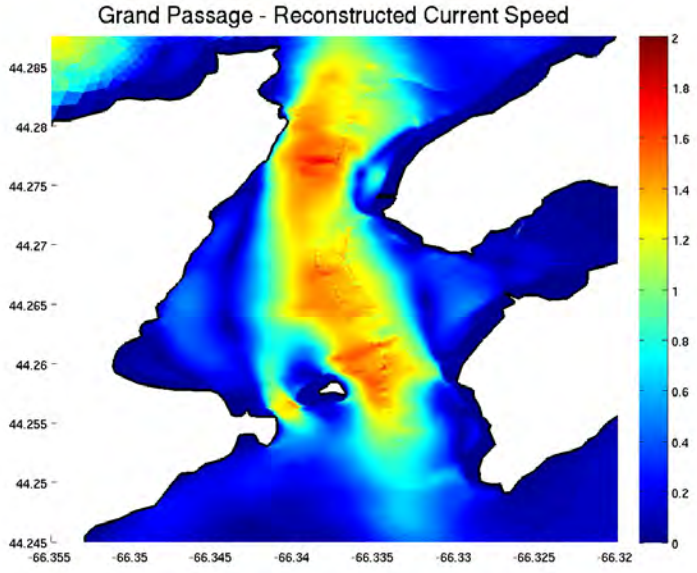

(b) Tidal Flow Speed

Figure 4.1: Grand Passage water velocities at one time step. (a) is the speed, (b) is the tidal flow speed reconstructed from the forcing tidal constituents.

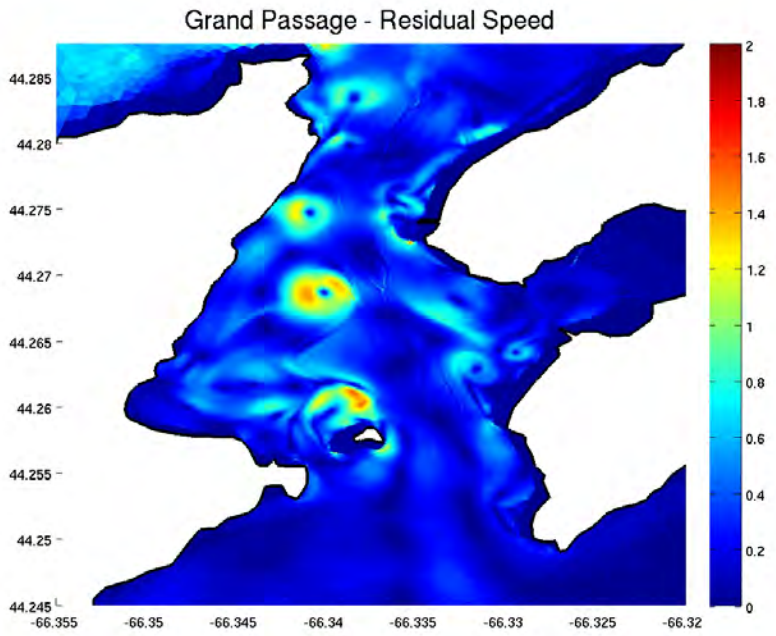

Figure 4.2: Grand Passage water intra-tidal/residual speed during a flood tide. The pattern of the residual speeds is typical of a vortex streak, generated by the water moving past Peter's Island.

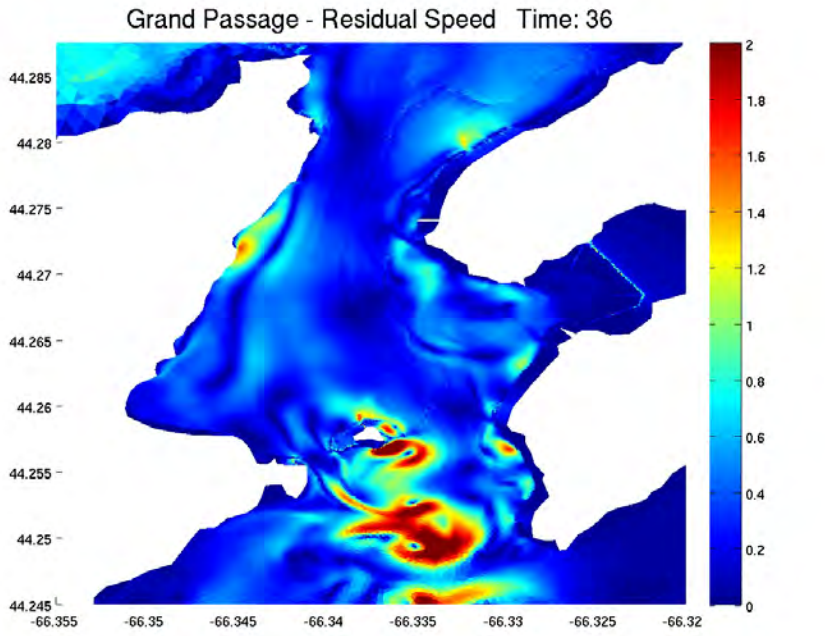

Figure 4.3: Grand Passage intra-tidal/residual speed during an ebb tide. Once again, a vortex streak is generated by Peter's Island, but now south of the island.

Chapter 5

Power Calculations using the Numerical Model

Using our numerical model, we examine the theoretical power that can be extracted form each passage in two ways. First, we plot spatial maps of the mean power density. These plots illustrate how the power density varies across each passage, and puts the numbers calculated at each specific ADCP location in perspective. Second, we plot the results of extracting power from a complete fence across each passage (following work in [Karsten et al., 2008]). In these plots we plot the power extracted versus the reduction in flow through the passage. The use of a complete turbine fence is not meant to model a realistic array of turbines. But this method can be used to estimate the total power that can be extracted from the flow and the resulting reduction of flow through the channel. Interpreting these power numbers as potential electricity generation must be done carefully (see [Karsten, 2012]). The true power potential and impact of a turbine array would require high resolution, 3D modelling that included a proper energy extraction and wake modelling that is beyond the scope of this report.

5.1 Results for Grand Passage

In Figure 5.1 we plot the mean power density for Grand Passage. The power density occasionally exceeds 6 kW/m^2, and has large areas between 3 and 6 kW/m^2. The ADCP at location 4 measured a mean power density of 3.39 kW/m^2 while the model predicted a slightly higher value of 3.82. ADCP location 2 also has a power density in the range of 3 kW/m^2.

Figure 5.2 shows the location of the turbine fence used to extract power in the numerical simulations. This fence has a blockage ratio of 1, that is, all the flow passes through the turbines. This is not meant to represent a realistic turbine farm, but is a simple way to determine the the potential power extraction and reduction of flow through the passage without having to model the details of a TEC. The power curve for Grand Passage, shown in Figure 5.3. The maximum power is 16 MW and a significant portion of this power can be extracted with only small changes in flow through the

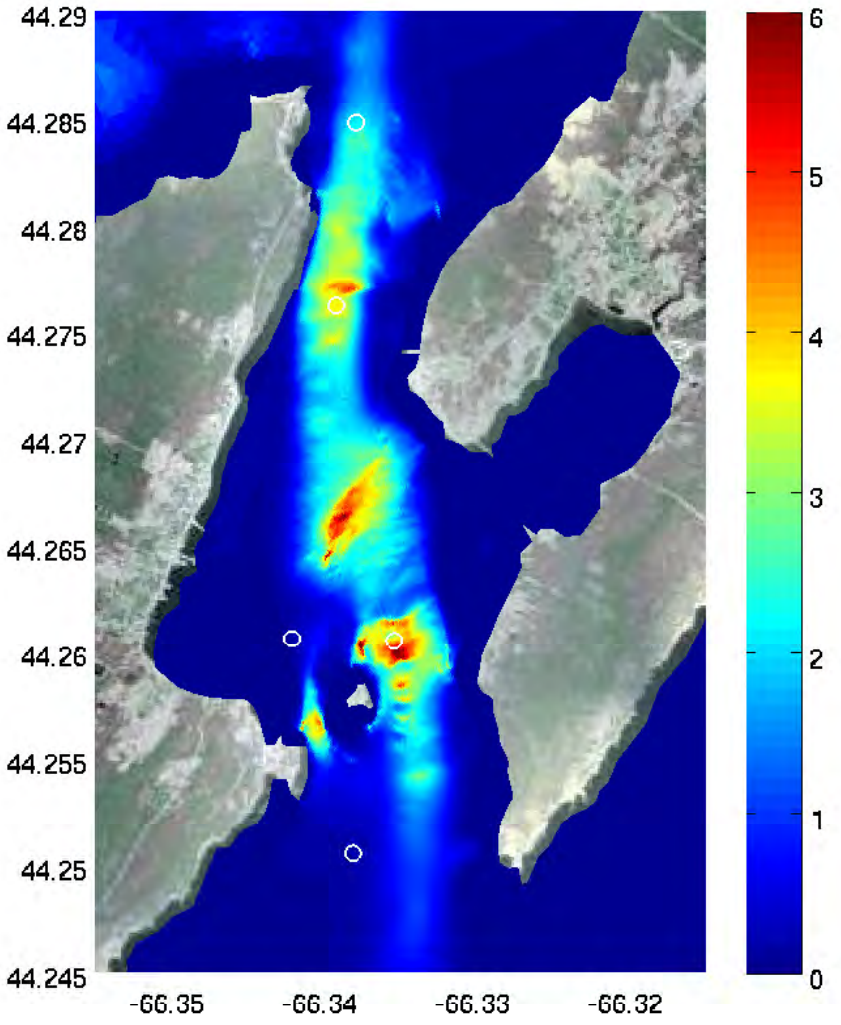

Figure 5.1: The mean power density in kW/m^2 for Grand Passage. The white circles are the locations of the ADCPs

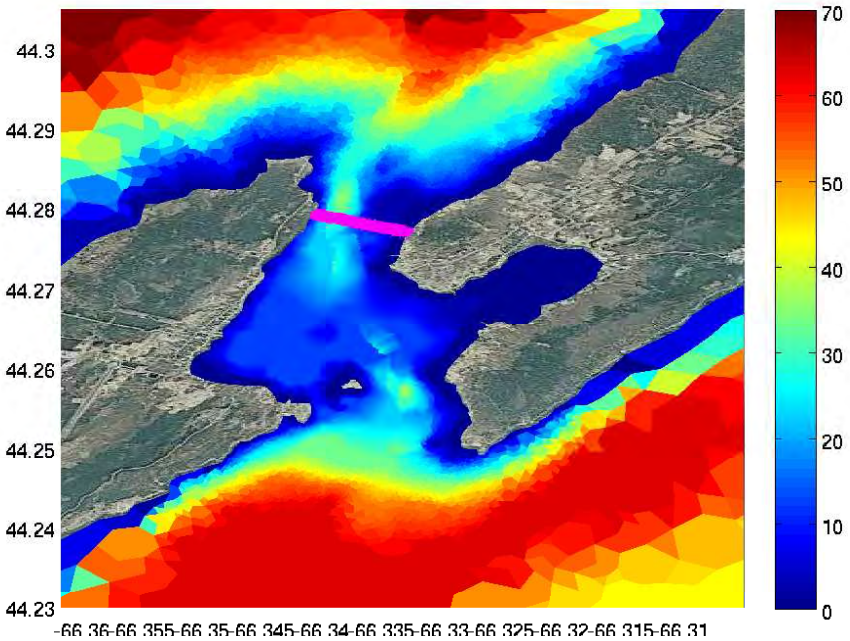

Figure 5.2: The bathymetry of Grand Passage used in the numerical simulations. The colours are the mean water depth in metres. The pink line is the location of the Grand Passage turbine fence.

passage. The flow through Grand Passage has little impact on the surrounding tides and it could be expected that a 10% reduction in flow will have little impact on surrounding intertidal zones.

5.2 Results for Petit Passage

In Fig.5.4 we plot the mean power density for Petit Passage. The mean power density routinely exceeds 8 kW/m^2 and reaches over 10 kW/m^2. These values suggest Petit Passage is an extremely energetic site. It should be noted that in comparison to the ADCP locations, the model is overestimating the power densities. For example, at the most energetic site, the model predicted a density of 7.99 compared to an ADCP value of only 5.86. Therefore the values shown in the spatial map are likely to be overestimates of the power density.

Fig. 5.5 shows the location of the turbine fence used to extract power in the numerical simulations. Fig.5.6 plots the extracted power versus reduction in flow for the Petit Passage turbine fence shown in Fig. 5.5. The maximum power is only 33 MW and significant portions of this power can be extracted with only small changes in flow

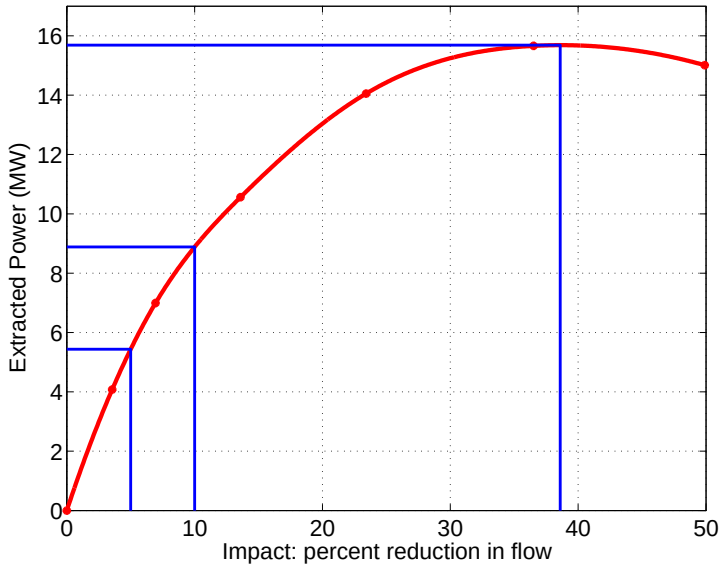

Figure 5.3: Grand Passage: Extracted power versus the reduction in flow through the turbine fence. The blue lines highlight the values presented in the Table 5.1. The dots are the values for the individual simulations, the curve is found using an interpolating spline.

through the passage. Since the flow through Petit Passage has little impact on the surrounding tides, it could be expected that a 10% or larger reduction in flow will have little impact on surrounding intertidal zones.

5.3 Results for Digby Gut

In Fig.5.7, we plot the mean power density for Digby Gut. The power density rarely exceeds 1.5 kW/m^2 and reaches a maximum of just over 2 kW/m^2 on the horseshoe shaped ridge where three of the ADCPs were located. The model values of the power density at the ADCP locations are roughly half the ADCP values, see Table 3.3. Therefore, the model may be underestimating the power density throughout the Gut. Around the horseshoe shaped ridge, the power density changes rapidly. This is likely related to rapid changes in the bathymetry in this region. Better resolution of this bathymetry may help explain the discrepancy between the ADCP and model velocities and power densities.

Fig. 5.8 shows the location of the turbine fence used to extract power in the numerical simulations. In Fig. 5.9, we plot the power extracted versus the reduction in the flow through Digby Gut. For a small passage, there is significant power that can be extracted

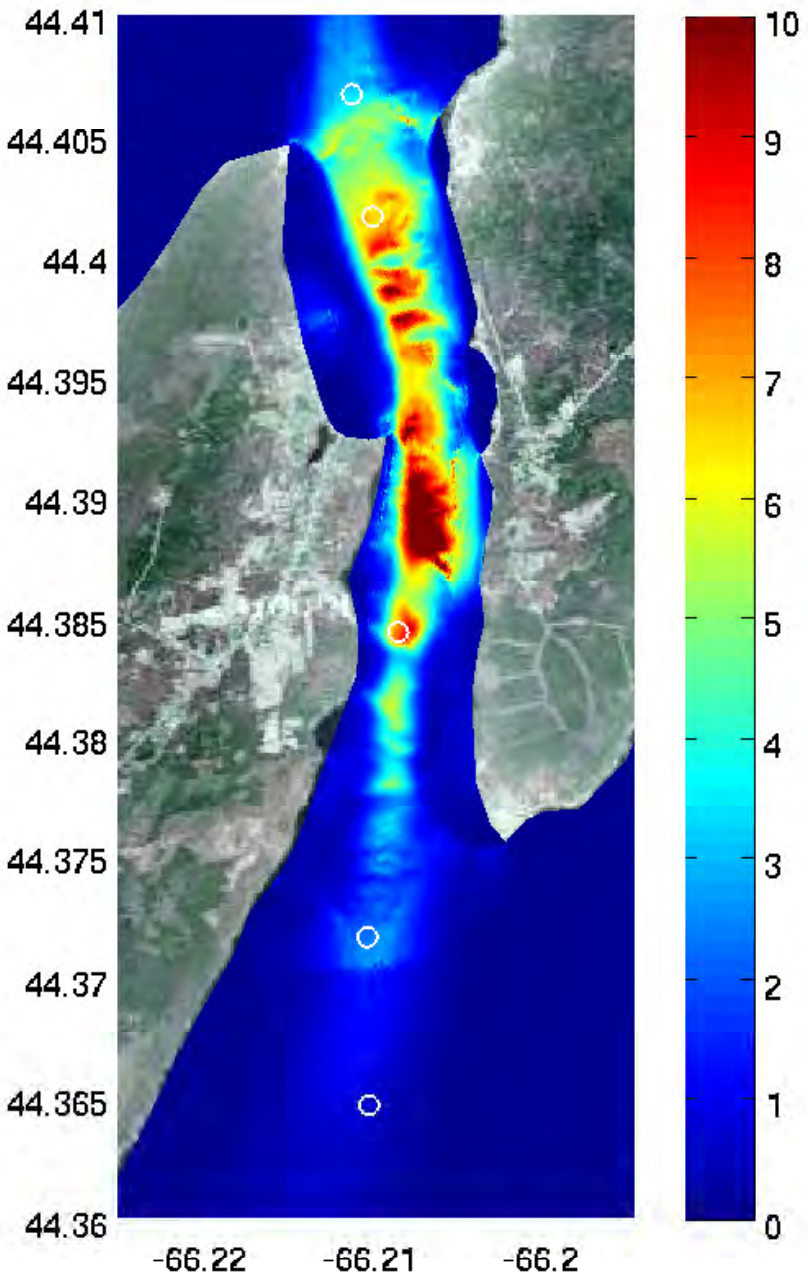

Figure 5.4: The mean power density in kW/m^2 for Petit Passage. The white circles are the locations of the ADCPs

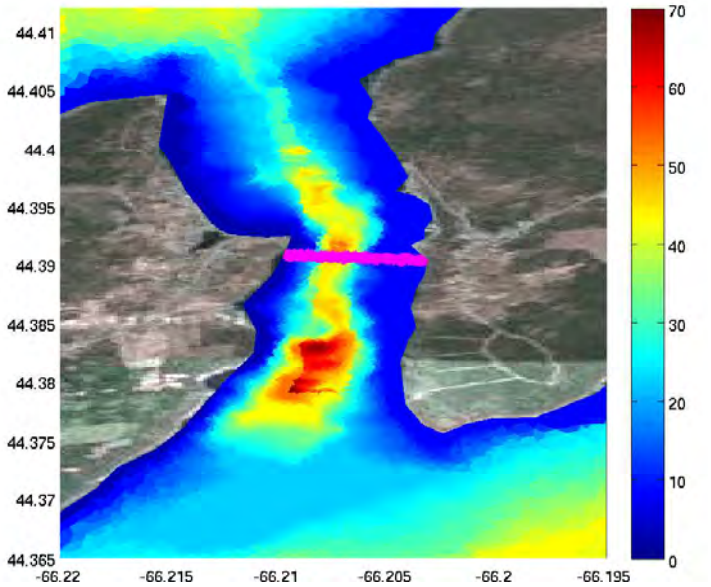

Figure 5.5: The mean water depth in metres of Petit Passage. The pink line is the location of the turbine fence.

and significant extractable power with only small changes in flow through the passage, see values in Table 5.1). As discussed elsewhere [Karsten et al., 2012], the potential power in Digby Gut is related to the significant potential energy of the tides in the Annapolis Basin. But, any reduction in the flow through Digby Gut will reduce the tidal range in Annapolis Basin.

Location	Maximum	10% Impact	5% Impact
Grand Passage	16	8.9 (55%)	5.4 (33%)
Petit Passage	33	19 (58%)	12 (36%)
Digby Gut	180	110 (58%)	67 (35%)

Table 5.1: Mean Power Extraction in MW. Impact is the reduction in flow through the passage. The percentages shown are the percentage of the maximum power that can be extracted at each impact level.

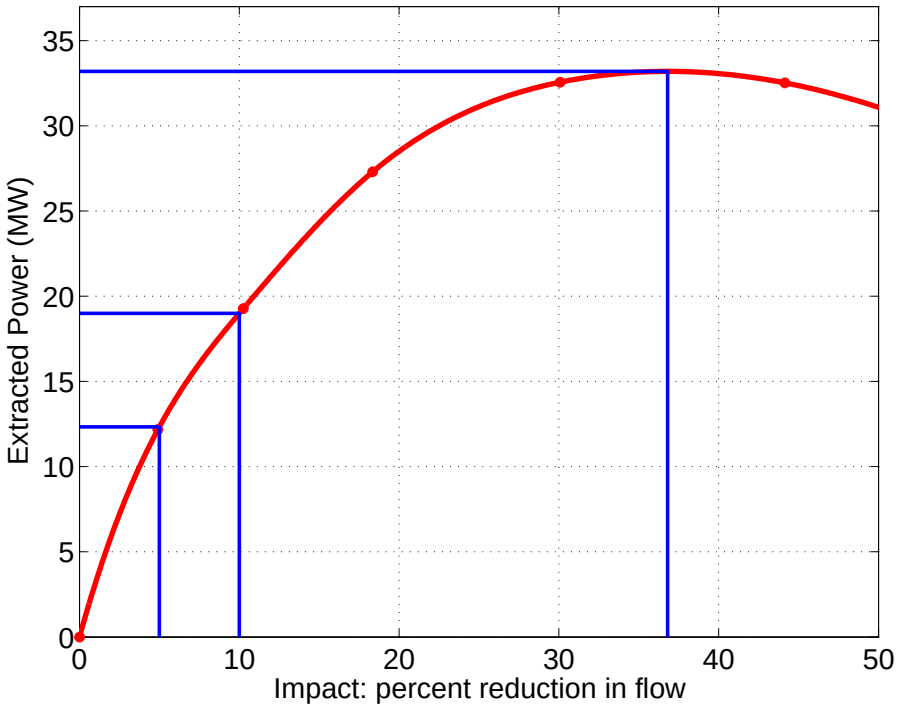

Figure 5.6: Extracted power versus the reduction in flow through the turbine fence for Petit Passage. The blue lines highlight the values presented Table5.1. The dots are the values for the individual simulations, the curve is found using an interpolating spline.

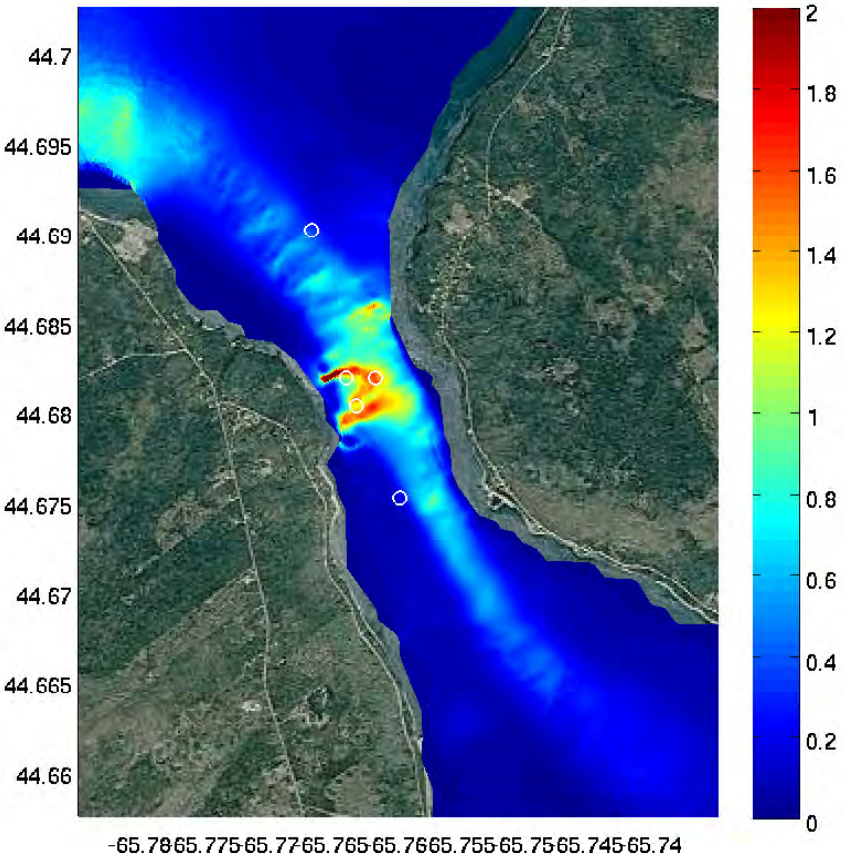

Figure 5.7: The mean power density in kW/m^2 for Digby Gut. The white circles are the locations of the ADCPs

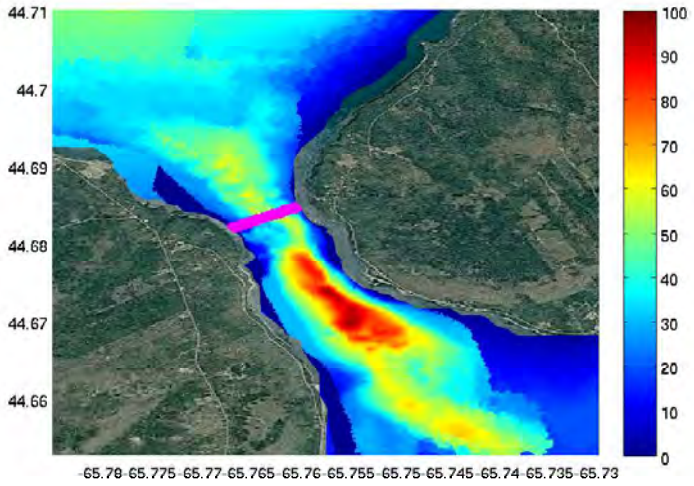

Figure 5.8: The mean water depth in metres of Digby Gut. The pink line is the location of the turbine fence.

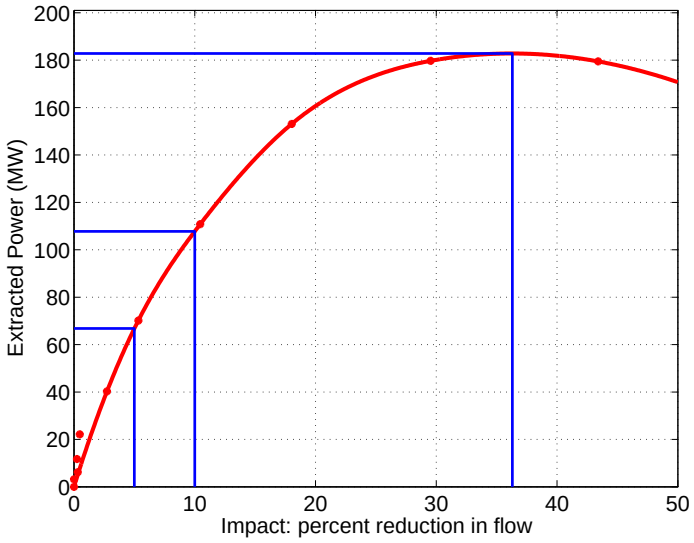

Figure 5.9: Extracted power versus the reduction in flow through the turbine fence for Digby Gut. The blue lines highlight the values presented in Table 5.1. The dots are the values for the individual simulations, the curve is found using an interpolating spline.

Chapter 6

Conclusions

In summary, the numerical model was greatly improved by increasing the resolution and using new bathymetric data in the three Digby Neck passages. This increase in resolution had important effects on the numerical simulations. It allowed the simulations to better model the tidal flow. But, more dramatically, it allowed the numerical model to better simulate the small scale details of the flow as it passed over and around bathymetric features. The flow pst bathymetry produces important variations in the flow, such as the eddies in the wake of Peter's Island in Grand Passage. When the model results are compared to the ADCP data, it is seen that the numerical model was modelling the tides and tidal currents well. The model also predicts flow variations at the same locations and times as the ADCPs. However, the model variations appear to be too large in magnitude, resulting in the prediction of maximum flow velocities much higher than that observed in the ADCP data. It is possible that this discrepancy could be eliminated by generating high-frequency numerical time series and taking appropriate averages of the data, in a manner similar to how the ADCP is analyzed. However, it should be noted that a hydrostatic, oceanographic model like FVCOM is not designed to correctly model the high frequency, 3D, non-hydrostatic velocity fluctuations seen in tidal races.

The modelled flow through Digby Gut did not agree as well with the ADCP data. The reason for this discrepancy is not fully understood. The project did not obtain new high resolution bathymetry for Digby Gut and Annapolis Basin, and this may mean the model is not as accurate in this region. Three of the Digby Gut ADCPs also moved during their deployment, so the ADCP data is not as reliable as in the other passages.

The improvements in the numerical model allow us to better understand the spatial and temporal variability in the tidal currents. The high resolution model allows us to connect the large fluctuations seen in the ADCP records to physical processes - eddies shed by Peter's Island and other bathymetric features. This establishes that these features are real, have large spatial scales, and must be considered when choosing sites for turbine deployment. Furthermore, the high resolution numerical model allows us to produce a detailed map of the power density for each passage. These maps show that the power density varies considerably in each passage with small regions of high power density. However, large fluctuations in flow velocity present in the model predictions and not observed in the ADCP data have a large effect on power density due to the cubic

relationship. Detailed investigation of regions of high power density is recommended to better characterize the turbulent flow that produces the flow speed fluctuations.

We also simulated power extraction from each of the passages using a complete turbine fence. This calculation is not as dependent on the grid resolution, but gives a theoretical power calculation based on the volume flux through the passage. The main results of this calculation is that Digby Gut has a much greater potential (60 MW) than Petit Passage (10–20 MW) or Grand Passage (5–10 MW). Digby Gut has such potential because the source of the power is the high tides in Annapolis Basin, while Petit and Grand Passage can only tap the much smaller tidal head across the passages. However, economical extraction of power from the relatively slow flow through Digby Gut presents a challenge.

Bibliography

C. Chen, R. C. Beardsley, and G. Cowles. An unstructured grid, finite-volume coastal ocean model (FVCOM) system. *Oceanography*, 19(1):78–89, 2006.

R. Karsten, M. O'Flaherty-Sproul, J. McMillan, J. Culina, G. Trowse, and A. Hay. Analysis of tidal turbine arrays in digby gut and petit passage, nova scotia. *Proceedings of the 4th International Conference on Ocean Energy*, 2012.

R. Karsten, A. Swan, and J. Culina. Assessment of arrays of in-stream tidal turbines in the bay of fundy. *Phil. Trans. R. Soc. A*, 371: 20120189, 2013. doi: http://dx.doi.org/10.1098/rsta.2012.0189.

R. H. Karsten. Tidal Energy Resource Assessment Map for Nova Scotia. *Report for OERA*, 2012. URL `http://www.oera.ca/marine-renewable-energy/tidal-research-projects/other-tidal-`

R. H. Karsten, J. M. McMillan, M.J. Lickley, and R. D. Haynes. Assessment of tidal current energy in the Minas Passage, Bay of Fundy. *Proc. IMechE Part A: J. Power and Energy*, 222:493–507, 2008.

R.H. Karsten. An assessment of the potential of tidal power from Minas Passage, Bay of Fundy, using three-dimensional models. *Proceedings of the 30th International Conference on Ocean, Offshore and Arctic Engineering, OMAE2011-49249*, 2011.

Rich Pawlowicz. Rich Pawlowicz's Matlab Stuff, 12 2001. Found at http://www.eos.ubc.ca/ rich/#T_Tide.